Adsorption (2015) 21:165–176
DOI 10.1007/s10450-015-9659-7

Mathematical modeling of the competitive sorption dynamics of acetone–butanol–ethanol on KA-I resin in a fixed-bed column

Pengfei Jiao · Jinglan Wu · Jingwei Zhou · Pengpeng Yang · Wei Zhuang · Yong Chen · Chenjie Zhu · Ting Guo · Hanjie Ying

Received: 16 October 2014 / Revised: 22 January 2015 / Accepted: 27 January 2015 / Published online: 11 February 2015

Abstract The recovery and purification of biobutanol based on the adsorption method were performed in dynamic conditions. Computational and theoretical modeling is an important tool in the characterization, development, and validation of fixed-bed columns. Relevant breakthrough curves provide valuable information for designing fixed-bed adsorption processes for field applications. In the present study, a general rate model (GRM), implementing convection/diffusion approach theory and a competitive isotherm model, was used to predict the competitive sorption dynamics of acetone–butanol–ethanol (ABE) on a KA-I resin in a fixed-bed column under different operating conditions, i.e., inlet feed flow rate, initial adsorbate concentration, and bed height. The model simulation was quantified by the absolute average deviation (AAD). The calculated AAD values, ranging from 0.05 to 0.1, indicated that the GRM gives a general prediction for experimental data. The axial dispersion, external mass transfer, and pore diffusion coefficients were calculated by a series of empirical correlations. Biot number was used to identify the rate controlling step for the adsorption process of ABE on the resin. And the pore diffusion coefficient was found to be major governing factor for adsorption of ABE. The data and modeling presented are valuable for designing the continuous chromatographic separation process and simulation of ABE.

Keywords Competitive adsorption · Breakthrough curve · Acetone–butanol–ethanol · General rate model · Rate controlling step

Pengfei Jiao and Jinglan Wu have contributed equally to this work.

P. Jiao · J. Wu (✉) · J. Zhou · P. Yang · W. Zhuang · Y. Chen · C. Zhu · T. Guo · H. Ying (✉)
College of Biotechnology and Pharmaceutical Engineering, Nanjing Tech University, Xin mofan Road 5, Nanjing 210009, People's Republic of China
e-mail: wujinglan@njtech.edu.cn

H. Ying
e-mail: yinghanjie@njtech.edu.cn

P. Jiao · J. Wu · J. Zhou · P. Yang · W. Zhuang · Y. Chen · C. Zhu · T. Guo · H. Ying
National Engineering Technique Research Center for Biotechnology, Nanjing 211816, People's Republic of China

J. Wu · J. Zhou · P. Yang · W. Zhuang · Y. Chen · C. Zhu · T. Guo · H. Ying
State Key Laboratory of Materials-Oriented Chemical Engineering, Nanjing 210009, People's Republic of China

Abbreviations

A_c	Cross-section area of the fixed-bed column (cm^2)
a	Competitive Langmuir isotherm constant (mL/g)
b	Competitive Langmuir isotherm constant (L/g)
Bi	Biot number
C	Concentration in the liquid phase (g/L)
$c_{i,p}$	Liquid phase concentration in the pore (g/L)
c_0	Initial adsorbate concentration (g/L)
C	Dimensionless concentration in the liquid phase
$C_{i,p}$	Dimensionless concentration in the pore
d_p	Particle size of the resin (cm)
D_{ax}	Axial dispersion coefficient (cm^2/min)
D_m	Molecular diffusivity (cm^2/min)
D_{pore}	Pore diffusion coefficient (cm^2/min)
k_{film}	External mass transfer coefficient (cm/min)
L_c	Length of the fixed-bed column (cm)
m	Mass of the used resin (g)
M_B	Molecular weight of water
Pe	Peclet number
$q_{i,p}$	Concentration in the stationary phase (mg/g)
Q_f	Volumetric flow rate of the liquid phase (mL/min)

r	Radial distance within the adsorbent particle (cm)
r_p	Particle radius (cm)
R	Dimensionless radial distance
St	Stanton number
t	Time (min)
$t_{1/2}$	Retention time (min), corresponding to half the initial adsorbate concentration
t_M	Dead time of the column (min), ($t_M = L_c/v$)
T	Operating temperature (K)
x	Axial coordinate (cm)
X	Dimensionless axial coordinate
U	Superficial flow velocity (cm/min)
V	Volume of the solution (mL)
$V_{i,A}$	Molar volume of adsorbate at normal boiling point[mL/(g mol)]

Greek symbols

φ	Association parameter (for water φ is given as 2.6)
ρ_p	Apparent density of the resin (g/mL)
ε_b	Bed porosity
ε_p	Particle porosity
v	Interstitial velocity of the liquid phase (cm/min), ($v = Q_f/(A_c\varepsilon_b)$)
η_B	Viscosity of solution (mpa s)
τ	Dimensionless time

Subscripts

A	Acetone
B	Butanol
E	Ethanol
i	Sorbate species
out	Outlet
t	Time

1 Introduction

In recent years, research into fermentation-derived butanol has gained renewed interest owing to the world's rapidly diminishing petroleum reserves, increasing environmental problems, and large amount of biomass available for inexpensive substrates (Nielsen and Prather 2009; Yen and Li 2011; Lin and Blaschek 1983). However, a major challenge in the economical production of biobutanol is its recovery and separation from the diluted fermentation broth (Saint Remi et al. 2011; García et al. 2009). Butanol recovery via conventional distillation is an energy-intensive process, especially when the concentration of the final product is very low (Saint Remi et al. 2011). Among alternative separation methods to recover butanol from fermentation broth, chromatographic separation based on adsorption has been shown to be a superior recovery technique that could be applied successfully in the energy-efficient removal of butanol from the fermentation broth in industrial applications (Nielsen and Prather 2009; Qureshi et al. 2005; Eom et al. 2013).

In the previous work, a porous resin KA-I has been demonstrated to adsorb butanol effectively and have a high affinity for butanol (Lin et al. 2012), the sorption dynamics of butanol on the resin KA-I in the single component system was investigated under different operating conditions (Lin et al. 2013). However, the acetone and ethanol, the main by-products in clostridial butanol fermentation, have a significant effect on butanol adsorption. Abdehagh et al. (2013) have investigated the effect of each component separately on butanol sorption on activated carbon. They found that the presence of acetone and ethanol did not affect butanol adsorption significantly. Oudshoorn et al. (2009) have studied multi-component adsorption isotherm of ABE on high-silica zeolite CBV 28014 and applied the ideal adsorbed solution theory model to describe the competitive adsorption behavior of ABE in synthetic mixture and filtered fermentation broth. And Eom et al. (2013) have also researched competitive adsorption isotherm of ABE on adsorbent resin using ideal adsorbed solution theory and developed competitive adsorption kinetic model based on the isotherm model. They all found that butanol had a higher affinity to the adsorbent and lower kinetic parameter value than the other components. Cousin Saint Remi et al. (2011, 2012) have investigated the competitive adsorption dynamics of ABE on a metal–organic framework ZIF-8 packed column. However, the analysis and modeling of relevant competitive adsorption breakthrough curves for different operating conditions with regard to inlet feed flow rate, adsorbent bed height, and initial adsorbate concentration have not been reported. Parameters like bed dimensions, resin weight, and inlet flow rate must be optimized for a given apparatus. Consequentially, mathematical models, once validated, can be frequently used to predict the dynamic performances of fixed-bed column systems and improve the column design in order to determine the optimal operating conditions (Lv et al. 2008).

Gu et al. (1990a) proposed a general rate model (GRM), which is considered to be the most realistic model for various multicomponent adsorption/desorption column processes. This model considers axial dispersion, film mass transfer, pore diffusion resistance, and nonlinear isothermal behaviors. Sulaymon and Ahmed (2008) have used this model to describe the multicomponent competitive adsorption behaviors of furfural and phenolic compounds in a fixed-bed column with activated carbon. The mathematical model provides a good fit to the experimental data. Lv et al. also used this model to simulate the adsorption breakthrough behaviors of Pb^{2+} in a fixed bed of ETS-10 adsorbent (Lv et al. 2008). A sensitivity analysis was

performed which showed the magnitude of the external mass transfer coefficient affected the initial breakthrough point in the breakthrough curves. Another chromatographic model in common use is based on the solid-film linear driving force approach (the so called LDF model), in which the film mass transfer and pore diffusion resistance are lumped into an effective mass transfer coefficient. This model is relatively simple and requires short computation times in comparison with the GRM. Kleinübing et al. (2012) have applied this model to simulate the adsorption dynamics in single and binary systems containing Cu(II) and Ni(II) ions using *Sargassum filipendula*. However, the LDF model has inherent weaknesses, as shown in multiple reports (Zhang and Ritter 1997; Buzanowski and Yang 1989; Goto and Hirose 1993; Zhou et al. 2013). For instance, when the adsorption isotherm is not very favorable, the LDF approximation is inapplicable (Zhang and Ritter 1997). Moreover, the values of effective mass transfer coefficient were usually determined by minimizing the difference between the predicted and measured effluent concentrations (Zhou et al. 2013), which means effective mass transfer coefficient was used as an adjustable parameter. Hence, the model would be not predictive.

Therefore, in the present work, the competitive breakthrough behaviors of ABE on the KA-I resin were experimentally measured and theoretically modeled using the GRM, which is a preliminary work of separation and purification of butanol based on continuous chromatographic separation technique in the future work. Influences of the operating conditions (inlet feed flow rate, initial adsorbate concentration, and adsorbent bed height) on the ABE competitive behavior were investigated. The model was evaluated by the absolute average deviation (AAD) between experimental and predicted effluent profiles. The model parameters, i.e., the axial dispersion, external mass transfer, and pore diffusion coefficients, were calculated using a series of empirical equations. External mass transfer and pore diffusion coefficients were evaluated and the rate controlling step was identified.

2 Mathematical model

2.1 General rate model (GRM)

The GRM is one of the most detailed chromatographic models, which in addition to the axial dispersion (D_{ax}) includes two additional mass transfer effects: (i) external mass transfer (k_{flim}) through the liquid film around an adsorbent particle and (ii) internal mass transfer governed by the solute diffusion into the pores of a particle (D_{pore}), which results in a radial concentration distribution inside the adsorbent particle (Gu et al. 1990a, b). In this model, the following assumptions were made in order to simplify the model complexity: (i) the resin is spherical in shape and uniform in size, (ii) the resin bed is homogeneous, (iii) the column void fraction is constant and the mobile phase velocity remains constant during a run, (iv) the chromatographic process conditions are isothermal, (v) the compressibility of the mobile phase is negligible, and (vi) the liquid phase has an axial dispersion flow.

2.1.1 Model equations

In fixed-bed experiments, the mathematical model was obtained by mass balancing a small section of a fixed-bed column bounded by an upper and lower surface with a distance of Δx as a controlled volume. Then, the flow was assumed to be one-dimensional along the flow direction based on the unit cross-sectional area. The details of the model equations are discussed elsewhere (Ghorai and Pant 2004) and are briefly discussed here. The following sections contain mathematical descriptions derived from mass balancing.

2.1.2 Mass balance in the liquid phase

Mass balance in the liquid phase of the adsorption column includes accumulation within the liquid, convection, axial dispersion, and external mass transfer through the liquid film outside the resin particles:

$$v\frac{\partial c_i}{\partial x}+\frac{\partial c_i}{\partial t}+\frac{1-\varepsilon_b}{\varepsilon_b}\frac{3}{r_p}k_{i,\text{film}}(c_i-c_{i,p}|_{r=r_p})=D_{i,ax}\frac{\partial^2 c_i}{\partial x^2}, \tag{1}$$

where v is the interstitial velocity of the liquid phase equal to $Q_f/(A_c\cdot\varepsilon_b)$, A_c is the cross-sectional area of column, Q_f is the volumetric flow rate, x is the axial position, t is the time, ε_b is the bed porosity obtained by determination of the void volume corresponding to the volume of deionized water required to brim the bed (Kleinübing et al. 2012), r is the radial distance within the adsorbent particle, r_p is the particle radius, $D_{i,ax}$ is the axial dispersion coefficient, $k_{i,\text{film}}$ is the external mass transfer coefficient, and c_i represents the concentration in the mobile phase, $c_{i,p}$ represents the liquid phase concentration in the pore.

Proper initial and boundary conditions are required to solve the second-order partial differential equations. For an initial clean fixed-bed column, the model equation obeys the following initial conditions:

$$0<x<L_c, t=0; \quad c_i=0. \tag{2}$$

A Danckwerts-type boundary condition at the bed inlet (Eq. 3) and constant flux at the bed outlet (Eq. 4) are appropriate for a fixed-bed adsorption process:

$$x=0(\text{inlet}), t>0; \quad D_{i,ax}\frac{\partial c_i}{\partial x}=v(c_i|_{x=0}-c_{i,0}) \tag{3}$$

$$x = L_c(\text{outlet}), t > 0; \quad \left.\frac{\partial c_i}{\partial x}\right|_{x=L_c} = 0. \tag{4}$$

2.1.3 The particle phase continuity equation in spherical coordinates

To model the diffusion of ABE molecules through the pore fluid, the intra pellet mass transfer equation is given as follows:

$$\varepsilon_p \frac{\partial c_{i,p}}{\partial t} + \rho_p \frac{\partial q_{i,p}}{\partial t} = \frac{1}{r^2}\frac{\partial}{\partial r}\left[r^2\left(\varepsilon_p D_{i,\text{pore}}\frac{\partial c_{i,p}}{\partial r}\right)\right], \tag{5}$$

where ε_p is the particle porosity, ρ_p is the apparent density of the resin, $D_{i,\text{pore}}$ is the pore diffusion coefficient, and $q_{i,p}$ represents the concentration in the stationary phase.

Initial conditions along with two additional boundary conditions, in the particle center and at the particle surface, are required, respectively, as follows:

$$t = 0; \quad c_{i,p} = q_{i,p} = 0 \tag{6}$$

$$r = 0,\ t > 0; \quad \left.\frac{\partial c_{i,p}}{\partial r}\right|_{r=0} = \left.\frac{\partial q_{i,p}}{\partial r}\right|_{r=0} = 0 \tag{7}$$

$$r = r_p,\ t > 0; \quad \varepsilon_p D_{i,\text{pore}}\left.\frac{\partial c_{i,p}}{\partial r}\right|_{r=r_p} = k_{i,\text{film}}(c_i - c_{i,p}|_{r=r_p}). \tag{8}$$

The equilibrium relationship between the solid and liquid concentration is represented by the competitive Langmuir isotherm model (Guiochon et al. 2006):

$$q_{i,p} = \frac{a_i c_{i,p}}{1 + \sum_j^N b_j c_{j,p}} \tag{9}$$

2.2 The dimensionless form of the GRM

To reduce the number of parameters and analyze their interdependence, it is recommended that the model equations as well as the initial and boundary conditions are converted into a dimensionless form. In the following definition of dimensionless variables, the initial adsorbate concentration $c_{i,0}$ is selected as a reference for the dimensionless concentrations and loadings:

$$C_i = c_i/c_{i,0} \tag{10}$$

$$C_{i,p} = c_{i,p}/c_{i,0} \tag{11}$$

$$Q_{i,p} = q_{i,p}/c_{i,0} \tag{12}$$

The dimensionless axial coordinate X of the column and radial coordinate R of each particle are obtained by division through the column length and particle radius, respectively:

$$X = x/L_c \tag{13}$$

$$R = r/r_p. \tag{14}$$

The dimensionless time τ is defined by the dead time t_M:

$$\tau = t/t_M; t_M = L_c/v. \tag{15}$$

Dimensionless parameters can be represented as follows:

$$Pe_i = v \cdot L_c/D_{i,ax} \tag{16}$$

$$St_i = \frac{3L_c \cdot k_{i,\text{film}}}{v \cdot r_p} \tag{17}$$

$$Bi_i = \frac{r_p \cdot k_{i,\text{film}}}{D_{i,\text{pore}} \cdot \varepsilon_p}, \tag{18}$$

where Pe is the Peclet number, St is the Stanton number, and Bi is the Biot number.

Substitution of Eqs. (10)–(18) into the GRM equations leads to the following dimensionless equations:

$$\frac{\partial C_i}{\partial \tau} + \frac{\partial C_i}{\partial X} + \frac{1-\varepsilon_b}{\varepsilon_b} \cdot St_i \cdot (C_i - C_{i,p}|_{R=1}) = (1/Pe_i) \cdot \frac{\partial^2 C_i}{\partial X^2} \tag{19}$$

$$\varepsilon_p \cdot \frac{\partial C_{i,p}}{\partial \tau} + \rho_p \cdot \frac{\partial Q_{i,p}}{\partial \tau} = St_i/(3Bi_i) \cdot \left(2/R \cdot \frac{\partial C_{i,p}}{\partial R} + \frac{\partial^2 C_{i,p}}{\partial R^2}\right). \tag{20}$$

The corresponding boundary conditions can be described as followed:

$$X = 0(\text{inlet}),\ \tau > 0; \quad 1/Pe_i \cdot \frac{\partial C_i}{\partial X} = C_i|_{X=0} - 1 \tag{21}$$

$$X = 1(\text{outlet}),\ \tau > 0; \quad \frac{\partial C_i}{\partial X} = 0 \tag{22}$$

$$R = 0,\ \tau > 0; \quad \frac{\partial C_{i,p}}{\partial R} = 0 \tag{23}$$

$$R = 1,\ \tau > 0; \quad \frac{\partial C_{i,p}}{\partial R} = Bi_i \cdot (C_i - C_{i,p}|_{R=1}). \tag{24}$$

The initial conditions at $\tau = 0$ become:

$$C_i = 0 \tag{25}$$

$$C_{i,p} = 0; \quad Q_{i,p} = 0. \tag{26}$$

The competitive Langmuir model in dimensionless form is as follows:

$$Q_{i,p} = \frac{a_i C_{i,p}}{1 + \sum_j^N b_j c_{j,0} C_{j,p}}. \tag{27}$$

2.3 Numerical solution

The partial differential equations were discretized into a set of ordinary differential equations using the orthogonal

collocation on finite elements method. After the discretization step, the ordinary differential equations with initial values were solved by the ordinary differential equation solver ODE23 in MATLAB 2010a. Absolute and relative tolerances of 10^{-5} were used.

2.4 Correlations of model parameters

The axial dispersion coefficient $D_{i,ax}$ can be calculated with the following empirical correlation(Suzuki and Smith 1971):

$$D_{i,ax} = 0.44D_{i,m} + 0.83Ud_p, \tag{28}$$

where U is the superficial flow velocity and d_p is the particle diameter. The molecular diffusivity $D_{i,m}$ of acetone, butanol, and ethanol were calculated using the Wilke–Chang correlation:

$$D_{i,m} = \frac{7.4 \times 10^{-8}(\varphi M_B)^{1/2}T}{\eta_B V_{i,A}^{0.6}}, \tag{29}$$

where φ is the association parameter, M_B is the molecular weight of water, T is the operating temperature, η_B is the viscosity of the solution, and $V_{i,A}$ is the molar volume of the adsorbate at its normal boiling point.

The external mass transfer coefficient $k_{i,\text{film}}$ can be calculated with the Wilson and Geankoplis correlation:

$$k_{i,\text{film}} = \frac{1.09}{\varepsilon_b}\frac{D_{i,m}}{d_p}\left(\frac{v \cdot d_p}{D_{i,m}}\right)^{1/3}. \tag{30}$$

The pore diffusion coefficient $D_{i,\text{pore}}$ can be estimated by the Mackie–Meares correlation:

$$D_{i,\text{pore}} = \frac{\varepsilon_\text{p}}{(2-\varepsilon_p)^2}D_{i,m}. \tag{31}$$

The absolute average deviation (AAD), defined in Eq. (31), is used to evaluate the model prediction. In general, an AAD value of less than 0.05 shows an almost perfect fit to the experimental data, an AAD value between 0.05 and 0.1 means the model provides a general agreement with the experimental data, and an AAD larger than 0.1 indicates the model may not truly correlate with the experimental data (Siahpoosh et al. 2009).

$$AAD = \frac{1}{N}\sum_{i=1}^{N}|C_{i,\text{exp}|X=1} - C_{i,\text{pre}|X=1}|, \tag{32}$$

where N is the number of experimental data points, $C_{i,\text{exp}|X=1}$ is the experimental dimensionless concentration at the bed outlet, and $C_{i,\text{pre}|X=1}$ is the dimensionless concentration at the bed outlet predicted by the model.

3 Materials and methods

3.1 Materials

3.1.1 Chemicals

The chemicals used in this work were all A.R. grade reagents, which were purchased from Sinopharm Chemical Reagent Co., Ltd. (Shanghai, China), and used without further purification. All solutions were prepared using deionized water.

3.1.2 Resin

The porous adsorption resin, KA-I, with a crosslinked—polystyrene framework was obtained from the National Engineering Technique Research Center for Biotechnology (Nanjing, China). The physicochemical properties of the resin are listed in Table 1. BET (Brunauer, Emmett, and Teller) and BJH (Barrett, Joyner, and Halenda) tests were performed to determine the surface area, pore volume, and pore size distribution of the resin.

3.1.3 Fermentation broth preparation

The ABE fermentation broth was produced by fermentation of glucose using *Clostridium acetobutylicum* B3 (CGMCC No. 5234) as the bacterial strain, which was previously isolated from soil and was selected after UV mutagenesis (Liu et al. 2013). The batch fermentation was conducted anaerobically in a 5-L serum bottle. The volume of the ABE production medium was 1.5 L, including 60 g/L glucose, 0.5 g/L K_2HPO_4, 0.5 g/L KH_2PO_4, 2.2 g/L CH_3COONH_4, 0.2 g/L $MgSO_4{\cdot}7H_2O$, 0.01 g/L $MnSO_4{\cdot}H_2O$, 0.01 g/L NaCl, 0.01 g/L $FeSO_4{\cdot}7H_2O$, 1 mg/L p-aminobenzoic acid, 1 mg/L thiamine, and 0.01 mg/L biotin. The fermentation broth was filtered by an

Table 1 Parameters of the KA-I resin and fixed-bed columns

Matrix structure	Polystyrene diethylbenzene
Crosslink density (%)	6.0
Functional group	Ester group
Polarity	Weakly polar
Average resin diameter, d_p (cm)	0.08
Porosity of resin, ε_p	0.65
Apparent resin density, (g/mL)	1.050
Skeletal resin density, ρ_s (g/mL)	0.700
BET specific surface area, S (m^2/g)	850–950
Pore volume, V_p (m^3/g)	0.62–0.66
Bed column porosity, ε_b	0.36
Cross-sectional area of column (cm^2)	7.065

ultrafiltration membrane unit (UOF4, Tianjin MOTIMO Membrane Technology Co., Ltd., Tianjin, China) to remove the microbial cells before it was used in the experiments.

3.2 Methods

3.2.1 Competitive adsorption equilibrium experiments

In the determination of multicomponent competitive adsorption isotherms, 100 mL Erlenmeyer flasks were filled with 50 mL of a known concentration of solutes and known weight of resin. The concentration ratio of acetone:butanol:ethanol in the mixture was equal to 3:6:1, which is close to the component ratio in a reported final fermentation broth (Liu et al. 2013). The flasks were then placed on a shaker and agitated continuously for 8 h at 298 K to attain equilibrium. Then, a sample was withdrawn from the supernatant fluid with a syringe and the concentration of the solute of interest was measured by gas chromatograph (GC) (Lin et al. 2013). The adsorbed amount was calculated by the following relationship:

$$q_{i,e} = \frac{(c_{i,0} - c_{i,e})V}{m}, \tag{33}$$

where $c_{i,0}$ and $c_{i,e}$ represent the initial and equilibrium aqueous concentration, respectively, of butanol (or other solute of interest), V is the volume of the solution, and m is the mass of the used resin.

3.2.2 Fixed-bed column experiments

The fixed-bed column experiments were carried out to evaluate the column performance in the separation of ABE ternary components by a KA-I resin. Experiments were conducted in a glass column (30 mm in diameter and 200 mm in length), which allows for a maximum amount of KA-I resin of about 100 g. The column was equipped with a water jacket connected to a super-heated water bath to keep the temperature constant. The fixed-bed operation was performed isothermally at 298 K ± 1 K and the feed stream (influent) containing the desired initial amount of ABE was packed into the KA-I resin column in a down-flow mode. Prior to each experiment, deionized water was passed through the column in an up-flow mode to remove air bubbles. The flow rate was controlled by a constant flow peristaltic pump (BT00-300M, Hebei, China). Samples were collected at the column outlet (effluent) at pre-determined time intervals and the concentration of ABE was periodically analyzed by GC. Effects of various experimental conditions, i.e., the inlet flow rate, initial ABE concentration, and adsorbent bed height, were investigated in the performance of competitive breakthrough for the adsorption of ABE onto the KA-I resin.

All experiments in this study were carried out at least three times and the experimental error was within 5–10 %. The reported values are the average of three data sets.

4 Results and discussion

4.1 ABE competitive adsorption isotherms

The competitive adsorption isotherms of acetone, butanol, and ethanol in the ternary system on a KA-I resin at 298 K along with the prediction curves calculated by the competitive Langmuir isotherm model (Eq. 9) are shown in Fig. 1. The corresponding Langmuir model parameters are given in Table 2. The simulation results fit the experimental data fairly well. Butanol has a high adsorption capacity on the KA-I resin, while acetone and ethanol are weakly adsorbed, especially ethanol. It can be observed in Fig. 1 that the ethanol is almost non-retained by the resin in the presence of butanol and acetone, which indicates the competitive adsorption phenomena exists in the ABE ternary mixture. The results are consistent to the report in the literature (Eom et al. 2013). The competitive adsorption will be further discussed in the following section.

4.2 ABE ternary mixture adsorption dynamics

4.2.1 Effect of inlet feed flow rate on the competitive ABE breakthrough curves

To investigate the adsorption performance of ABE in the column at different inlet feed flow rates, the adsorbent bed

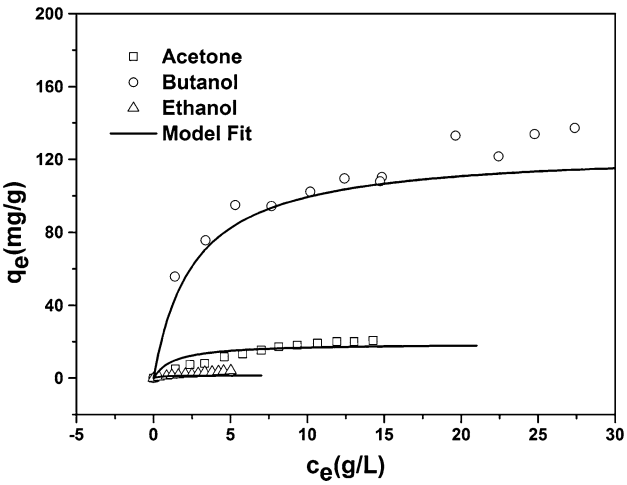

Fig. 1 Competitive adsorption isotherms of acetone, butanol, and ethanol in the ternary system

Table 2 Multicomponent competitive adsorption isotherm parameters for ABE on KA-I resin

Solute	a (mL/g)	b (L/g)	D %[a]
Acetone	14.5	0.15	8.9
Butanol	48.0	0.30	9.1
Ethanol	3.6	0.05	7.8

[a] D %, the average absolute percent deviations. $D\,\% = \frac{1}{N}\sum\left|\frac{q_{\exp}-q_{\mathrm{pre}}}{q_{\exp}}\right| \times 100\,\%$

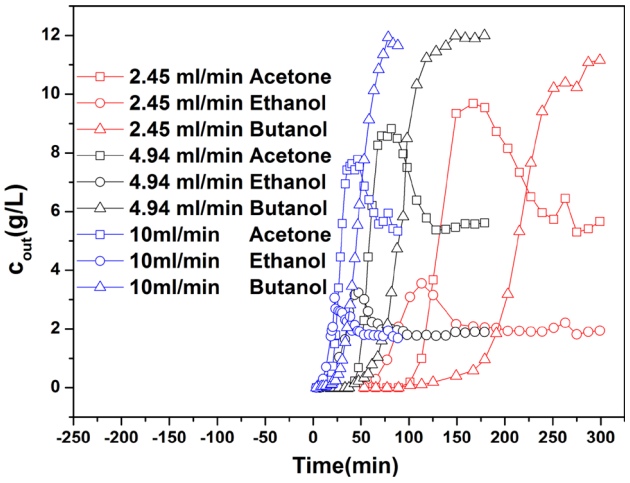

Fig. 2 Effect of inlet feed flow rate on the competitive breakthrough curves of ABE adsorption on a KA-I resin ($c_{A,0} = 6.0$ g/L, $c_{B,0} = 12.0$ g/L, $c_{E,0} = 2.0$ g/L, $L_c = 10.2$ cm, $H/D = 3.4$, $T = 298$ K $\pm$ 1 K)

height was fixed at 10.2 cm and the initial ABE concentration in the feed was held constant at 6.0, 12.0, and 2.0 g/L, respectively, while the inlet feed flow rate was changed from 2.45 to 10.0 mL/min. The breakthrough curves of ABE for $c_{i,\mathrm{out},t}$ versus time at various inlet feed flow rates are shown in Fig. 2. It is interesting to observe from Fig. 2 that overshoots exist in the concentration profiles of ethanol and acetone, which is evidence of the competitive adsorption (Ghorai and Pant 2004). The adsorbed ethanol and acetone (the weakly retained substance) are displaced by butanol (the strongly adsorbed component), which corresponds to the results of the ABE adsorption isotherms (see Fig. 1). The breakthrough point decreases at a higher flow rate. A higher flow rate reduces the time that the adsorbates are in contact with the adsorbent, thus allowing less time for adsorption to occur, leading to an early breakthrough of the adsorbates. The result is consistent with the results of Ahmad and Hameed (2010). Moreover, as can be seen in Fig. 2, when the inlet flow rate increases from 2.45 to 10 mL/min, the shape of concentration profiles of acetone and ethanol becomes more flat. According to Sulaymon and Ahmed (2008), a probable explanation for the phenomenon is that the rate of competitive adsorption will decrease with the increase of Biot number for each solute, which leads to less displacement of weak retained components by strongly retained component. In our case, the Biot number for each adsorbate increases with the increase of inlet flow rate (see Table 3). Therefore, less ethanol and acetone are displaced by butanol at a high inlet flow rate, thus more flat breakthrough profiles of the acetone and ethanol are observed. The flat concentration profiles and early breakthrough point will lead to the difficult separation of ABE. However, the low flow rate will lead to the long operating time needed for separation. Therefore, an appropriate flow rate needs to be selected to satisfy the separation.

4.2.2 *Effect of initial adsorbate concentration on the competitive breakthrough curves*

The breakthrough curves of ABE with different initial concentrations are depicted in Fig. 3. The ratio of the ABE ternary mixture was the same as that in the fermentation broth. The inlet feed flow rate was kept at 5.0 mL/min and the adsorbent bed height was 10.2 cm. Figure 3 shows that the concentration profiles of ABE become steeper with increasing feed concentration. This phenomenon can be explained by the fact that the driving force depends on the concentration gradient of the solute and can be improved by using a higher initial concentration to create a larger concentration difference (Volesky and Prasetyo 1994; Zhou et al. 2013). Moreover, an interesting phenomenon can be seen in Table 3 where the retention time ($t_{1/2}$) of the ABE concentration profiles increases with reduction of the initial feed concentration. By increasing the initial ABE concentration from 3.0, 6, 1 g/L to 9.0, 18.0, 3.0 g/L, the $t_{1/2}$ of ABE decreased by 47.3, 54.4, and 34.2 %, respectively. This phenomenon is typical for convex isotherms, i.e., Langmuir type. For isotherm of the langmuir-type, the retention time of each adsorbate decreases with its increasing concentration in the feed solution, when the concentration is located in the nonlinear range of the adsorption isotherm (Schmidt-Traub 2005). In our case, the concentrations of ABE under investigation are located in the nonlinear range of the competitive adsorption isotherms (see Fig. 1). Therefore, the retention times of ABE decreased with the increase of its initial concentrations in the feed solution.

4.2.3 *Effect of adsorbent bed height on the competitive breakthrough curves*

The competitive adsorption behaviors of ABE were investigated at adsorbent bed heights of 4.2, 10.2, and 18.0 cm. The inlet flow rate was fixed at 5 mL/min and the initial ABE concentrations were 6.0, 12.0, and 2.0 g/L, respectively. The experimental breakthrough curves at different adsorbent bed heights are plotted in Fig. 4. It can

Table 3 Experimental conditions for the column runs and parameters for prediction of the breakthrough curves of ABE

	Run 1	Run 2	Run 3	Run 4	Run 5	Run 6	Run 7	Run 8
Q_f (mL/min)	2.45	4.94	10.0	4.94	4.94	4.94	4.94	4.94
Concentration of feed solution (g/L)								
Acetone	6.0	6.0	6.0	6.0	6.0	3.0	9.0	6.18
Butanol	12.0	12.0	12.0	12.0	12.0	6.0	18.0	10.48
Ethanol	2.0	2.0	2.0	2.0	2.0	1.0	3.0	1.2
L_c (cm)	10.2	10.2	10.2	4.2	18.0	10.2	10.2	10.2
Aspect ratio *H/D*	3.4	3.4	3.4	1.4	6.0	3.4	3.4	3.4
ε_b	0.36	0.36	0.36	0.36	0.36	0.36	0.36	0.36
t_M (min)	10.59	5.25	2.59	2.16	9.27	5.25	5.25	5.25
$D_{\text{Acetone},ax}$ ($\times 10^{-2}$ cm^2/min)	2.34	4.68	9.43	4.68	4.68	4.68	4.68	4.68
$D_{\text{Butanol},ax}$ ($\times 10^{-2}$ cm^2/min)	2.33	4.67	9.43	4.67	4.67	4.67	4.67	4.67
$D_{\text{Ethanol},ax}$ ($\times 10^{-2}$ cm^2/min)	2.34	4.68	9.44	4.68	4.68	4.68	4.68	4.68
$t_{1/2}$ (min) Experimental								
Acetone	122.6	55.3	24.6	19.2	101.2	84.8	44.7	53.0
Butanol	219.0	98.3	46.6	36.2	189.5	167.8	76.6	97.1
Ethanol	77.3	32.6	15.3	10.3	67.6	41.2	27.1	24.5
Pore diffusion coefficient $D_{i,\text{pore}}$ ($\times 10^{-4}$ cm^2/min)								
Acetone	2.73	2.73	2.73	2.73	2.73	2.73	2.73	2.73
Butanol	2.23	2.23	2.23	2.23	2.23	2.23	2.23	2.23
Ethanol	3.12	3.12	3.12	3.12	3.12	3.12	3.12	3.12
External mass transfer coefficient $k_{i,\text{film}}$ (cm/min)								
Acetone	0.14	0.17	0.22	0.17	0.17	0.17	0.17	0.17
Butanol	0.12	0.15	0.19	0.15	0.15	0.15	0.15	0.15
Ethanol	0.15	0.19	0.24	0.19	0.19	0.19	0.19	0.19
Peclet number								
Acetone	421	424	425	174	748	424	424	424
Butanol	422	424	425	175	749	424	424	424
Ethanol	420	423	425	174	747	423	423	423
Biot number (*Bi*)								
Acetone	31.6	38.3	49.6	38.3	38.3	38.3	38.3	38.3
Butanol	33.1	41.4	52.4	41.4	41.4	41.4	41.4	41.4
Ethanol	29.6	37.5	47.3	37.5	37.5	37.5	37.5	37.5
AAD	0.090	0.097	0.070	0.054	0.043	0.120	0.086	0.076

be observed from Fig. 4 that the shape of the concentration profiles of ethanol and acetone becomes sharp with the increasing height of the bed. According to Sulaymon and Ahmed (2008), the behavior can be explained by the increase of competitive displacement of weak adsorbed components (ethanol and acetone) by strongly adsorption component (butanol), which is caused by the increasing Peclet number. In our case, the Peclet number of ABE increased with the increase of bed height (see Table 3). As shown in Table 3, the ABE retention time $t_{1/2}$ increased with increasing adsorbent bed height as expected, because a larger bed height corresponds to a larger amount of adsorbent in the column, and more active sites are available for sorption of the adsorbate with the increase of adsorbent bed height. Therefore, more time is needed to saturate all the adsorbent in the fixed bed. In addition, as the bed height increased, the $t_{1/2}$ difference between butanol and the other two solutes became larger, indicating that more efficient separation of ABE can be attained by increasing the bed height.

4.3 Mathematical modeling for adsorption behaviors of ABE ternary system

The GRM was used to predict the competitive adsorption dynamics of ABE. The experimental and predicted breakthrough curves of ABE ternary system at different operating conditions (inlet feed flow rate, initial adsorbate concentration, and adsorbent bed length) were shown in Fig. 5 simultaneously. The AAD values between 0.5 and

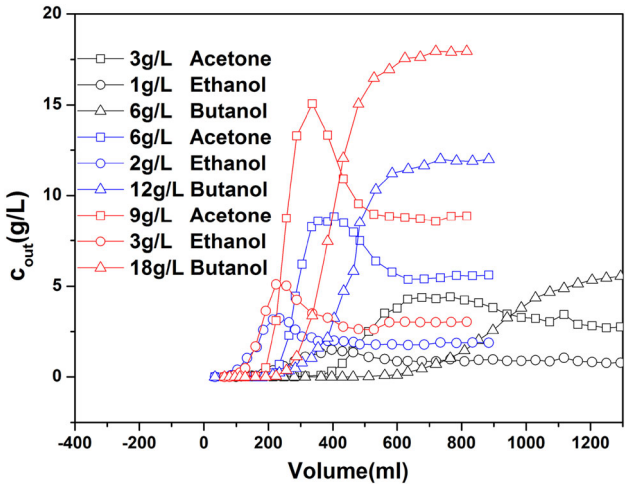

Fig. 3 Effect of initial adsorbate concentration on the competitive breakthrough curves of ABE adsorption on a KA-I resin ($Q_f = 5.0$ mL/min, $L_c = 10.2$ cm, $H/D = 3.4$, $T = 298$ K $\pm$ 1 K)

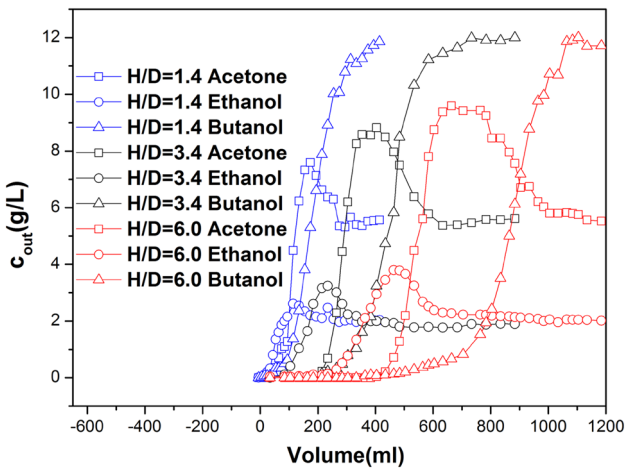

Fig. 4 Effect of adsorbent bed height on the competitive breakthrough curves of ABE adsorption on a KA-I resin ($c_{A,0} = 6.0$ g/L, $c_{B,0} = 12.0$ g/L, $c_{E,0} = 2.0$ g/L, $Q_f = 5.0$ mL/min, $T = 298$ K $\pm$ 1 K)

1.0 indicated that the GRM could provide a general description to the competitive adsorption behaviors of ABE at different operating conditions. Axial dispersion, external mass transfer, and pore diffusion coefficients were determined by Eqs. (28), (30), and (31), respectively. The results were given in Table 3. The values of external mass transfer coefficient were found to be in the range of 0.14–0.22, 0.12–0.19, and 0.15–0.24 cm/min for ABE, respectively. It could be observed that the values of k_{film} varied with different flow rates but kept constant for different initial adsorbate concentrations. According to Guiochon et al. (2006), k_{film} increases with the decrease of film mass transfer resistance. The film mass transfer resistance is related with the thickness of liquid film outside the resin particles. At a higher flow rate, film mass transfer resistance decreases as liquid film outside the resin particles becomes thinner caused by the increasing turbulence. Therefore, the external mass transfer coefficient k_{film} increases with increasing flow rates. However, k_{film} was almost independent of initial adsorbate concentrations. The k_{film} is determined by hydrodynamic conditions and mainly depends on fluid velocity for specific adsorbate-adsorbent system. The fluid velocity is constant for all the concentration ranges under investigation. Therefore, the values of k_{film} remain constant for different initial feed concentration.

A single value of D_{pore} was found to be used in the modeling of breakthrough curves over the operating range of feed flow rates, initial adsorbate concentrations, and adsorbent bed length. The same phenomenon had been reported by many other researchers. Ponnusami et al. (2010) have reported a concentration–independent internal diffusion coefficient for the adsorption of methylene blue onto plant leaf powders. Quek and Al-Duri (2007) have applied a single value of intraparticle diffusion coefficient to predict the concentration profiles of lead ion on coir for various operating conditions. However, the values of D_{pore} for ABE were variant to each other. The values were 2.73×10^{-4}, 2.23×10^{-4}, and 3.12×10^{-4} cm^2/min for ABE, respectively. The D_{pore} values were specific to each adsorption system. Physicochemical properties of solutes including size, polarity, and solubility may affect the pore diffusivities when the same adsorbent was used (Wu et al. 2009). The Biot number (Bi) was calculated by Eq. (18), and the results were shown in Table 3. Bi measures the relative rate between external mass transfer and internal diffusion. Adsorption is governed by external mass transfer ($Bi < 10$), intraparticle mass transfer ressistance ($Bi > 10$), or both ($Bi \sim 10$) (Kumar et al. 2014). From Table 3, it can be observed that the values of Bi at different operating condition are all more than 10, indicating that pore diffusion is the rate controlling step for the adsorption process of ABE on the resin. The phenomenon can be probably due to pore structure of the resin. According to the IUPAC definition of pore diameters, the KA-I resin contains mesopore (2 nm < pore size < 50 nm) and micropore (pore size < 2 nm) regions simultaneously (see Fig. 6). The diffusion of the ABE in the pore may be limited by the specific pore structure of the resin.

4.4 Competitive adsorption dynamics of ABE from the actual fermentation broth

The column experiment was carried out with the actual ABE fermentation broth used as a feed solution (see Run 8 in Table 3). The concentrations of ABE in the fermentation broth were 6.18, 10.48 and 1.2 g/L, respectively. The Langmuir isotherm constants (a_i and b_i) and axial dispersion, external mass transfer, and pore diffusion coefficient from prediction of ABE model broth were used in the actual fermentation broth prediction directly (see Table 3).

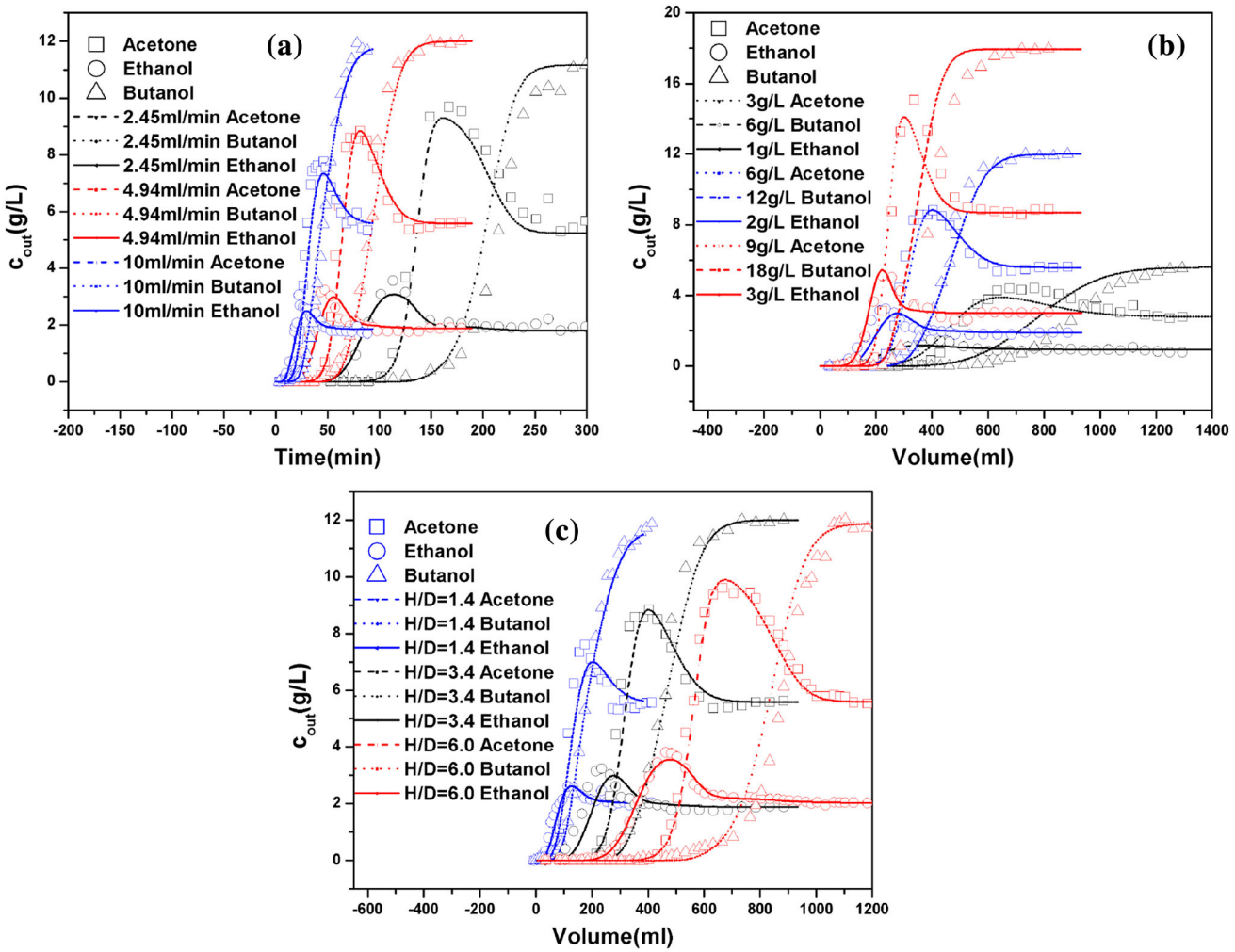

Fig. 5 Experimental and predicted breakthrough curves of ABE on KA-I resin at different operating conditions (**a** inlet feed flow rate; **b** initial adsorbate concentration; **c** adsorbent bed height). The *dash lines*, *dot lines*, and *solid lines* represent the predicted breakthrough curves

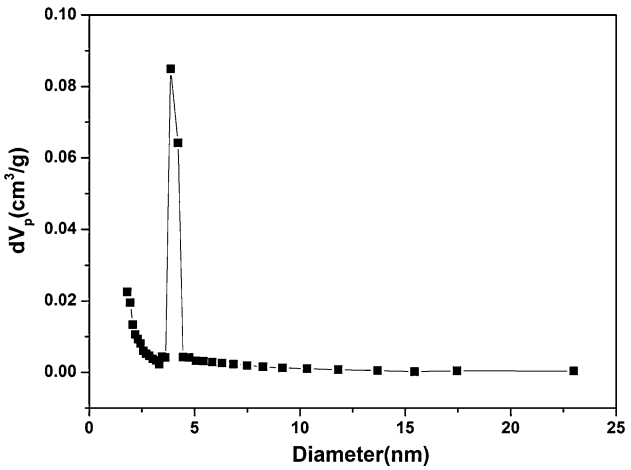

Fig. 6 Pore diameter distribution of the KA-I resin

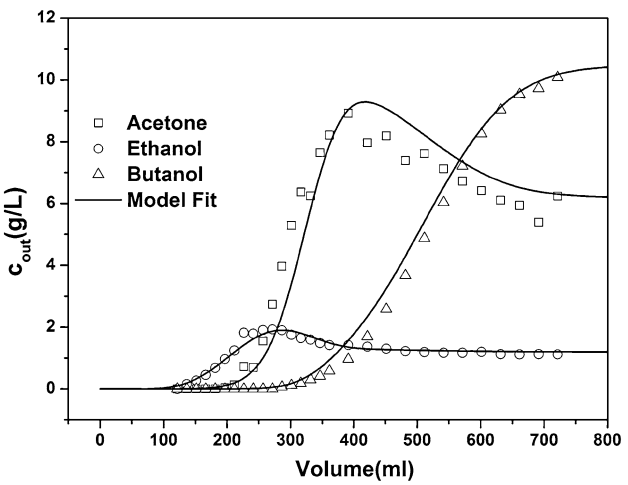

Fig. 7 Experimental and predicted competitive adsorption breakthrough curves of ABE using the actual fermentation broth as feed

The experimental ABE breakthrough curves were shown in Fig. 7. Meanwhile, the GRM model prediction was presented in Fig. 7 as well. The value *AAD* was 0.076, which indicating that the model could provide a general description to the breakthrough curve of ABE from actual the fermentation broth. Moreover, the result also proved that other compounds in the actual fermentation broth had almost no disturbance to the adsorption of ABE.

5 Conclusions

The shape and retention time of ABE have been found to be affected by the inlet feed flow rate and bed height, which need to be selected appropriately to satisfy the separation of ABE in dynamic conditions. The general rate model (GRM) has been successfully used to describe and predict the multicomponent competitive adsorption behaviors of ABE in a packed bed under different operating conditions. Three important model parameters, namely the axial dispersion coefficient $D_{i,ax}$, external mass transfer coefficient $k_{i,\text{film}}$, and pore diffusion coefficient $D_{i,\text{pore}}$, have been calculated by several empirical correlations. The AADs between 0.05 and 0.1 demonstrate the rationality of the calculation based on the empirical correlations. The values of *Bi* at different operating conditions are all more than 10, indicating that pore diffusion is the rate controlling step for the adsorption process of ABE on the resin. Based on the excellent results, the proposed model can be applied to design and fabricate devices and develop separation optimization methods to further industrial production. Undoubtedly, the desorption process of ABE from the resin should also be investigated experimentally and theoretically in the future work in order to realize the continuous separation of ABE.

Acknowledgments This work was supported by Program for Changjiang Scholars and Innovative Research Team in University (PCSIRT), National Outstanding Youth Foundation of China (Grant No.: 21025625), 473000, 12KJB530003, 21306086, National High-Tech Research and Development Plan of China (863 Program, 2012AA021202) and Project Funded by the Priority Academic Program Development of Jiangsu Higher Education Institutions (PAPD).

References

Abdehagh, N., Tezel, F.H., Thibault, J.: Adsorbent screening for biobutanol separation by adsorption: kinetics, isotherms and competitive effect of other compounds. Adsorption **19**(6), 1263–1272 (2013). doi:10.1007/s10450-013-9566-8

Ahmad, A.A., Hameed, B.H.: Fixed-bed adsorption of reactive azo dye onto granular activated carbon prepared from waste. J. Hazard. Mater. **175**(1–3), 298–303 (2010). doi:10.1016/j.jhazmat.2009.10.003

Buzanowski, M.A., Yang, R.T.: Extended linear driving-force approximation for intraparticle diffusion rate including short times. Chem. Eng. Sci. **44**(11), 2683–2689 (1989). doi:10.1016/0009-2509(89)85211-X

Eom, M.-H., Kim, W., Lee, J., Cho, J.-H., Seung, D., Park, S., Lee, J.H.: Modeling of a biobutanol adsorption process for designing an extractive fermentor. Ind. Eng. Chem. Res. **52**(2), 603–611 (2013). doi:10.1021/ie301249z

García, M., Sanz, M.T., Beltrán, S.: Separation by pervaporation of ethanol from aqueous solutions and effect of other components present in fermentation broths. J. Chem. Technol. Biotechnol. **84**(12), 1873–1882 (2009). doi:10.1002/jctb.2259

Ghorai, S., Pant, K.K.: Investigations on the column performance of fluoride adsorption by activated alumina in a fixed-bed. Chem. Eng. J. **98**(1–2), 165–173 (2004). doi:10.1016/j.cej.2003.07.003

Goto, M., Hirose, T.: Approximate rate equation for intraparticle diffusion with or without reaction. Chem. Eng. Sci. **48**(10), 1912–1915 (1993). doi:10.1016/0009-2509(93)80362-T

Gu, T., Tsai, G.-J., Tsao, G.T.: New approach to a general nonlinear multicomponent chromatography model. AIChE J. **36**(5), 784–788 (1990a). doi:10.1002/aic.690360517

Gu, T., Tsao, G.T., Tsai, G.-J., Ladisch, M.R.: Displacement effect in multicomponent chromatography. AIChE J. **36**(8), 1156–1162 (1990b). doi:10.1002/aic.690360805

Guiochon, G., Felinger, A., Shirazi, D.G., Katti, A.M.: Fundamentals of Preparative and Nonlinear Chromatography. Elsevier, Amsterdam (2006)

Kleinübing, S.J., Guibal, E., da Silva, E.A., da Silva, M.G.C.: Copper and nickel competitive biosorption simulation from single and binary systems by *Sargassum filipendula*. Chem. Eng. J. **184**, 16–22 (2012). doi:10.1016/j.cej.2011.11.023

Kumar, P., Lau, P.W., Kale, S., Johnson, S., Pareek, V., Utikar, R., Lali, A.: Kafirin adsorption on ion-exchange resins: isotherm and kinetic studies. J. Chromatogr. A **1356**, 105–116 (2014). doi:10.1016/j.chroma.2014.06.035

Lin, X., Li, R., Wen, Q., Wu, J., Fan, J., Jin, X., Qian, W., Liu, D., Chen, X., Chen, Y., Xie, J., Bai, J., Ying, H.: Experimental and modeling studies on the sorption breakthrough behaviors of butanol from aqueous solution in a fixed-bed of KA-I resin. Biotechnol. Bioproc. E. **18**(2), 223–233 (2013). doi:10.1007/s12257-012-0549-5

Lin, X., Wu, J., Fan, J., Qian, W., Zhou, X., Qian, C., Jin, X., Wang, L., Bai, J., Ying, H.: Adsorption of butanol from aqueous solution onto a new type of macroporous adsorption resin: studies of adsorption isotherms and kinetics simulation. J. Chem. Technol. Biot. **87**(7), 924–931 (2012). doi:10.1002/jctb.3701

Lin, Y.-L., Blaschek, H.P.: Butanol production by a butanol-tolerant strain of *Clostridium acetobutylicum* in extruded corn broth. Appl. Environ. Microbiol. **45**(3), 966–973 (1983)

Liu, D., Chen, Y., Li, A., Ding, F., Zhou, T., He, Y., Li, B., Niu, H., Lin, X., Xie, J., Chen, X., Wu, J., Ying, H.: Enhanced butanol production by modulation of electron flow in *Clostridium acetobutylicum* B3 immobilized by surface adsorption. Bioresour. Technol. **129**, 321–328 (2013). doi:10.1016/j.biortech.2012.11.090

Lv, L., Zhang, Y., Wang, K., Ray, A.K., Zhao, X.S.: Modeling of the adsorption breakthrough behaviors of Pb^{2+} in a fixed bed of ETS-10 adsorbent. J. Colloid Interface Sci. **325**(1), 57–63 (2008). doi:10.1016/j.jcis.2008.04.067

Nielsen, D.R., Prather, K.J.: In situ product recovery of n-butanol using polymeric resins. Biotechnol. Bioeng. **102**(3), 811–821 (2009). doi:10.1002/bit.22109

Oudshoorn, A., van der Wielen, L.A.M., Straathof, A.J.J.: Adsorption equilibria of bio-based butanol solutions using zeolite. Biochem. Eng. J. **48**(1), 99–103 (2009). doi:10.1016/j.bej.2009.08.014

Ponnusami, V., Rajan, K.S., Srivastava, S.N.: Application of film-pore diffusion model for methylene blue adsorption onto plant leaf powders. Chem. Eng. J. **163**, 236–242 (2010). doi:10.1016/j.cej.2010.07.052

Quek, S.Y., Al-Duri, B.: Application of film-pore diffusion model for the adsorption of metal ions on coir in a fixed-bed column. Chem. Eng. Process. **46**(5), 477–485 (2007). doi:10.1016/j.cep.2006.06.019

Qureshi, N., Hughes, S., Maddox, I.S., Cotta, M.A.: Energy-efficient recovery of butanol from model solutions and fermentation broth by adsorption. Bioprocess. Biosyst. Eng. **27**(4), 215–222 (2005). doi:10.1007/s00449-005-0402-8

Saint Remi, J.C., Remy, T., Van Hunskerken, V., van de Perre, S., Duerinck, T., Maes, M., De Vos, D., Gobechiya, E., Kirschhock, C.E., Baron, G.V., Denayer, J.F.: Biobutanol separation with the metal-organic framework ZIF-8. ChemSusChem **4**(8), 1074–1077 (2011). doi:10.1002/cssc.201100261

Saint Remi, J.C., Baron, G., Denayer, J.: Adsorptive separations for the recovery and purification of biobutanol. Adsorption **18**(5–6), 367–373 (2012). doi:10.1007/s10450-012-9415-1

Schmidt-Traub, H.: Preparative Chromatography of Fine Chemicals and Pharmaceutical Agents. Wiley-Vch, Weinheim (2005)

Siahpoosh, M., Fatemi, S., Vatani, A.: Mathematical modeling of single and multi-component adsorption fixed beds to rigorously predict the mass transfer zone and breakthrough curves. Iran. J. Chem. Chem. Eng. **28**(3), 25–44 (2009)

Sulaymon, A.H., Ahmed, K.W.: Competitive adsorption of furfural and phenolic compounds onto activated carbon in fixed bed column. Environ. Sci. Technol. **42**(2), 392–397 (2008). doi:10.1021/Es070516j

Suzuki, M., Smith, J.M.: Axial dispersion in beds of small particles. Chem. Eng. J. **3**, 256–264 (1971)

Volesky, B., Prasetyo, I.: Cadmium removal in a biosorption column. Biotechnol. Bioeng. **43**(11), 1010–1015 (1994). doi:10.1002/bit.260431103

Wu, F.-C., Tseng, R.-L., Juang, R.-S.: Initial behavior of intraparticle diffusion model used in the description of adsorption kinetics. Chem. Eng. J. **153**(1–3), 1–8 (2009). doi:10.1016/j.cej.2009.04.042

Yen, H.-W., Li, R.-J.: The effects of dilution rate and glucose concentration on continuous acetone–butanol–ethanol fermentation by *Clostridium acetobutylicum* immobilized on bricks. J. Chem. Technol. Biot. **86**(11), 1399–1404 (2011). doi:10.1002/jctb.2640

Zhang, R., Ritter, J.A.: New approximate model for nonlinear adsorption and diffusion for single particle. Chem. Eng. Sci. **52**(18), 3161–3172 (1997). doi:10.1016/S0009-2509(97)00124-3

Zhou, J., Wu, J., Liu, Y., Zou, F., Wu, J., Li, K., Chen, Y., Xie, J., Ying, H.: Modeling of breakthrough curves of single and quaternary mixtures of ethanol, glucose, glycerol and acetic acid adsorption onto a microporous hyper-cross-linked resin. Bioresour. Technol. **143**, 360–368 (2013). doi:10.1016/j.biortech.2013.06.009